Available online at www.sciencedirect.com
ScienceDirect
Catalysis Today 123 (2007) 245–256
CATALYSIS TODAY
www.elsevier.com/locate/cattod

Au–TiO_2 catalysts on carbon nanofibres prepared by deposition-precipitation and from colloid solutions

Nina Hammer [a], Ingvar Kvande [a], Xin Xu [b], Vidar Gunnarsson [c], Bård Tøtdal [c], De Chen [a], Magnus Rønning [a,*]

[a] *Department of Chemical Engineering, Norwegian University of Science and Technology (NTNU), N-7491 Trondheim, Norway*
[b] *Beijing Institute of Petrochemical Technology, Daxing 102617, Beijing, China*
[c] *Department of Physics, NTNU, N-7491 Trondheim, Norway*

Available online 6 April 2007

Abstract

Au catalysts have been prepared (i) on TiO_2, (ii) on carbon nanofibres (CNF) and (iii) on TiO_2 deposited onto CNF. Catalysts prepared from deposition-precipitation (DP) and from colloid solutions have been characterised using XRD, TEM, TGA and XAS and tested in the water–gas shift (WGS) reaction. DP yields large Au particles (>50 nm) on CNF-containing supports. High Au dispersion on carbon nanofibres requires preparation via other methods such as colloid formation. Au particle growth is more pronounced during the synthesis steps than during thermal treatments. This increase is not observed for the Au particles on TiO_2 but only when CNF is present, indicating that the surface properties of TiO_2 are altered by the CNF. TiO_2 XANES analyses show that distortions in the lattice symmetry of TiO_2 are introduced when the oxide is deposited on CNF. The distortion of the TiO_2 structure by the CNF may also introduce changes that promote the turnover frequencies. The WGS activity significantly improves when titania is present. This shows that coexistence of Au and TiO_2 is needed to obtain high catalytic activity in the WGS reaction, indicating that the active sites are either on the Au–TiO_2 interface or that the reaction follows a bifunctional mechanism.

Keywords: Au catalyst; TiO_2; Carbon nanofibres; Water–gas shift reaction; Deposition-precipitation; Au colloids

1. Introduction

Nanoparticles of gold supported on metal oxides have been shown to be very active catalysts for several reactions such as CO oxidation [1] and the water–gas shift (WGS) reaction [2]. The preparation of finely dispersed gold particles is believed to be a crucial step in obtaining highly active gold catalysts for the reactions. Several methods have been applied to prepare nanoparticles of Au on different supports, such as deposition-precipitation (DP) with urea or NaOH [3], aqueous impregnation [4], deposition of Au sol [5,6], flame spray pyrolysis [7] and co-precipitation [8,9]. The preparation route is critical for the Au–support interaction and for obtaining the required metal particle dispersion.

DP is the most common method for preparing highly active Au/TiO_2 catalysts, usually by deposition of $[AuO_x(OH)_{4-2x}]^{n-}$ species on the support [10]. DP is carried out by exposing the support to an aqueous solution of $HAuCl_4$. The pH is increased by addition of a base and heating leads to the formation of an oxidic precursor on the support. Moreau et al. [11] have investigated the deposition of Au on TiO_2, with the initial pH of the $HAuCl_4$ solution set at different values. They found that a pH of about 9 was optimal for obtaining high CO oxidation activity. At this pH the main species in the solution were anionic Au complexes where most of the chlorine had been removed by hydrolysis. The amount of Au deposited decreased progressively as the final pH was raised above 8. A dynamic equilibrium between the adsorbed species and the solution is established, which is shifted towards the solution side as the pH is increased. As a result, changes in the pH will influence the amount of Au deposited as well as particle sizes and hence catalytic activity. It is suggested that if the pH is kept below 6–7 during the synthesis, the support surface and/or the adsorbed complexes can still retain some chloride ions, which are promoting mobility and aggregation of the particles. Excessive particle growth can be avoided by increasing the pH.

* Corresponding author. Tel.: +47 73 59 41 21; fax: +47 73 59 50 47.
E-mail address: ronning@chemeng.ntnu.no (M. Rønning).

0920-5861/$ – see front matter
doi:10.1016/j.cattod.2007.03.001

Deposition of highly dispersed gold on carbon is not a trivial task due to the tendency towards agglomeration of the metal particles. In addition to metal particle size, the catalyst activity and stability are also controlled by the structure and morphology of the support materials. The selection of an efficient support is thus a decisive factor to provide the desired contact between the gold particles and the substrate [12]. Controlling the Au particle size before deposition on carbon is essential. A number of different synthesis methods of Au colloids are reported in literature. The synthesis methods employ different reducing agents, which lead to various particle sizes and size distributions. The use of sodium citrate as a reducing agent is a common method for preparing Au colloids [13]. The method yields colloids fairly uniform in size with diameters in the range of 15–20 nm. The reduction of chloroauric acid with tetrakis(hydroxymethyl)phosphonium chloride (THPC) in a partially hydrolysed form gives an average particle size of about 2 nm [14]. The first reduction step of Au(III) by THPC is the generation of the active reducing agent tris(hydroxymethyl)phosphine. The formation of gold colloids is believed to proceed via gold nucleation centres with further gold atoms being attached to these centres. The reaction time required for the formation of the Au sol is depending on the adding sequence of the reagents. The use of different volumes of chloroauric acid solution and ageing time of the reducing mixture (NaOH, THPC) also has a marked impact on the outcome of the reaction [14,15].

Highly dispersed gold is regarded as a potentially useful material for various industrial and environmental applications [16]. A wide range of oxide support materials have been investigated for the WGS reaction, including TiO_2 [17–19], ZnO [20], ZrO_2 [21], CeO_2 [2,22,23] and Fe_2O_3 [24,25]. The stability of Au supported on Fe_2O_3 in particular is limited due to the tendency of agglomeration of gold particles. This is probably related to a reduction in total surface area by transforming γ-Fe_2O_3 to α-Fe_2O_3 and Fe_3O_4 [24]. Gold supported on CeO_2 doped with La or Ga [2,26,27] and promoted with various elements [28] have been studied for the water–gas shift (WGS) reaction in order to improve the activity and stability of the catalysts.

The WGS reaction is a key step in fuel processing to generate pure H_2 for fuel cell applications. In such applications a successful catalyst needs to possess high activity as well as good structural stability at pertinent conditions. Andreeva et al. [29] reported that Au enhances the catalytic activity of iron oxide for the WGS reaction and that the activity is comparable with that of a conventional copper based catalyst. Sakurai et al. [17] have reported catalytic activity for Au/TiO_2 where the turnover frequency was four times higher at 100 °C than for a commercial $Cu/ZnO/Al_2O_3$ catalyst. Comparable CO conversion rates to commercial catalysts were obtained with Au loadings in the range of 5–10 at.%. Fu et al. [30] have reported that the activity is higher for Au/CeO_2 compared to Au/TiO_2. Sakurai et al. [31] have also studied the same reaction in a stream of CO, CO_2, H_2O, H_2 and He. Au/CeO_2 had a much higher activity than Au/TiO_2, Pt/CeO_2 and a commercial $Cu/ZnO/Al_2O_3$ at temperatures below 250 °C where the CO conversion was close to equilibrium. The Au/CeO_2 catalysts maintained 100% selectivity to CO_2 up to 350 °C.

Carbon nanofibres (CNF) have been used in the present work to disperse and stabilise the TiO_2 support and hence the Au particles. The use of CNF as support material in heterogeneous catalysis has attracted growing interest due to their specific characteristics. The CNF are resistant to acid/base media and the precious metals can easily be recovered by burning off the support [32]. The size and morphology of the CNF provide high surface areas while maintaining macroscopic pore sizes and hence good transport properties in the reactor, and reduced risk of micropore-induced diffusion limitations. Bulushev et al. [33] showed that gold nanoparticles of 2–5 nm supported on woven fabrics of activated carbon fibres were effective for CO oxidation at room temperature. Gold catalysts on carbon supports are so far most commonly used for liquid reactions, such as oxidation of alcohols and sugar [34].

The scope of the present work is to examine how the physical and chemical properties of the Au particles are influenced by the choice of support material and synthesis methods. The catalysts have been studied by various characterisation techniques and tested in the WGS reaction. The changes in the structure of Au and TiO_2 for different pre-treatments have been investigated by X-ray absorption spectroscopy (XAS). The Au catalysts have been prepared by DP with urea and deposition of Au from colloid solutions on different supports. The supports used are TiO_2, CNF, and TiO_2 deposited on CNF. The results show that the properties obtained from the synthesis methods are highly dependent on the choice of support material.

2. Experimental

2.1. Catalyst preparation

CNF were synthesized in a fixed-bed reactor at 600 °C using a Ni–hydrotalcite derived catalyst. The catalyst was reduced at 600 °C for 4 h in H_2/N_2 (25/75 ml/min) before reaction. CH_4/H_2 (160/40 ml/min) was used as the reaction gas mixture [35].

Before deposition of the metals, the CNF were treated in acid to remove the Ni catalyst from the preparation. This method also introduces surface functional groups, which act as anchoring sites for the catalyst precursors. CNF were refluxed in concentrated nitric acid for 1 h followed by filtration, washing in distilled water until stable pH (close to 6) and dried in an oven at 100 °C for 12 h. The acid treatment was performed twice.

The catalysts supported on CNF have been prepared in two steps; first deposition of the TiO_2 onto the CNF followed by deposition of gold. The amount of titania deposited is 10 wt.% of the total catalyst. For both preparation methods, the amount of gold in the solution corresponds to a gold loading of 2 wt.% of the total catalyst. The supports were weighed before any treatment. Since the treatments may lead to weight-loss in the materials, loadings of more than 2 wt.% were measured for some of the catalysts.

TiO_2 was prepared by hydrolysis of a $TiCl_4$ solution by adding polyethylene imine (PEI) to the solution. The mixture was covered with aluminium foil and kept at 70 °C in an oven. After 40 min the white precipitate began to appear and the CNF were added. The mixture was stirred and refluxed at 70 °C for another 2 h. The suspension was filtrated, washed with ethanol and dried for 12 h at 100 °C. A more detailed description of this preparation procedure is given by Sun et al. [36].

DP was performed in excess urea. The support was dispersed in distilled water and a 43 mM $HAuCl_4$ solution was added together with urea. The pH was adjusted to 2 by adding 1 M HNO_3 and the solution was heated to 90 °C. The decomposition of urea led to a gradual rise in pH from 2 to 7. The solution was filtrated and washed with ethanol until no Cl^- was detected in the filtrate by precipitation with $AgNO_3$.

The Au sol was prepared by reduction of chloroaurate(III) ions in a partially hydrolysed THPC solution following the procedure reported by Duff et al. [37]. 0.2 M NaOH and THPC (1.2 ml of 80 wt.% THPC in water diluted to 100 ml) was added to the required amount of continuously stirred distilled water. After 2 min a 43 mM $HAuCl_4$ solution was added. Dispensing the gold(III) solution into the alkaline THPC mixture yielded a rapid colour change from yellow to dark orange-brown indicating formation of the gold sol. The support was dispersed in 50 ml water and the Au sol was added dropwise. The pH was adjusted to 2 by adding 0.2 M HNO_3 and the solution was stirred for 1 h. The mixture was filtrated and no colour could be observed in the filtrate. The same washing procedure as stated above was performed.

All catalysts were dried in an oven at 100 °C for 12 h and treated in flowing nitrogen for 2 h at 250 °C.

2.2. Characterisation

Thermogravimetric analysis in oxidising atmosphere (TGA) was used to study the crystallinity of the CNF [38]. In addition, TGA gives an indication of the amount of metal residue after purification and the amount of Au and TiO_2 deposited onto the CNF. TGA analyses were carried out using a Perkin-Elmer Thermogravimetric Analyzer (TGA7). The samples were heated to 900 °C at a heating rate of 10 °C/min in air. The air flow was 80 ml/min.

Elemental analysis (X-ray fluorescence, XRF) was performed on some of the samples to verify the sample composition.

X-ray powder diffraction (XRD) analyses of the samples were preformed using a Siemens D5005 with Cu Kα radiation. The crystal size of Au and TiO_2 was calculated from the line broadening using the Scherrer equation. XRD measurements were performed after each preparation step.

Nitrogen adsorption measurements were performed in a SA 3100 Surface Area Analyzer from Beckman Coulter. Prior to N_2 adsorption measurements, the samples were degassed at 150 °C for 3 h. The specific surface area was calculated by the Brunauer–Emmett–Teller (BET) method. The *t*-plot method was applied to calculate the micropore volume and micropore surface area.

Transmission electron microscopy (TEM) and scanning transmission electron microscope/energy dispersive spectroscopy (STEM/EDS) in high angle annular dark field (HAADF) mode was used to study the sample morphology and to obtain particle sizes and size distributions. The average particle size was obtained from TEM images by counting approximately 500 particles per sample. The analyses were performed on a JEOL 2010F electron microscope with an acceleration voltage of 200 kV. The sample powder was suspended in chloroform using an ultrasonic bath. The sample was spread onto a Cu-grid coated with holey carbon film.

The zeta potential was measured as a function of the pH on a Malvern 3000HS Zetasizer connected to a titrator (Malvern instruments). The samples were diluted in a 0.01 M NaCl solution. The pH was adjusted with 0.5 M NaOH and 0.5 M HCl. The electrophoretic mobility was measured with a laser Doppler velocimeter. The zeta potential was determined by the Smoluchowski approximation [39] in the pH range from 2 to 12 with three repetitions.

UV–vis spectra of the Au sol were recorded by a Shimadzu UV-240 spectrophotometer in the wavelength range of 900–190 nm. Two commercial colloid solutions of known particle sizes (5 nm and 10 nm, from Ted Pella Inc.) were also measured for comparison.

Au L_{III} edge (11,919 eV) XAS data were collected at the Swiss-Norwegian Beamlines (SNBL), European Synchrotron Radiation Facility (ESRF), France. Spectra were recorded using a channel-cut Si(1 1 1) monochromator. Higher order harmonics were rejected by means of a chromium-coated mirror to give a cut-off energy of approximately 17 keV. The beam current ranged from 160 mA to 200 mA at 6.0 GeV. The data were collected in fluorescence mode using a 13 element solid state detector. A Lytle type environmental cell [40] was used for various *in situ* treatments of some of the samples. An Au foil (thickness 3 μm) was used for energy calibration during the experiments. The catalysts were heated to 300 °C in flowing 5% O_2/He, 5% H_2/He or pure He and held for 2 h. Extended X-ray absorption fine structure (EXAFS) data were collected for the gold nanoparticles on the two supports at room temperature prior to and after the thermal treatment. Scans of the edge profiles of the Au L_{III} edge were collected during the treatments.

Ti K edge (4774 eV) XAS data were collected *ex situ* at beam line 11.1 at the ELETTRA Laboratory, Italy. Spectra were collected in transmission mode using a double Si(1 1 1) crystal monochromator. The beam current ranged from 80 mA to 340 mA at 2.0 GeV. A Ti foil (thickness 4 μm) was used for energy calibration during the experiments.

The XAS data analysis program WinXAS 3.1 [41] was used for background subtraction and normalisation of the spectra. Model fitting was carried out with the EXCURV98 program using curved-wave theory and *ab initio* phase shifts [42,43]. During the least squares fitting procedure it is important to minimise correlation effects between the parameters that strongly affects the EXAFS oscillations. Therefore, the EXAFS spectra were least squares fitted in k space using k^0 and k^2 weighted data. An Au metal foil, $HAuCl_4$ and AuCl were used

as model compounds to check the validity of the *ab initio* phase shifts and establish the general amplitude reduction factor (AFAC). During the analysis, the spectra were Fourier filtered (1.5–3.5 Å) to suppress contributions from distant shells. The model was obtained from the filtered spectra before the final fitting of the model was checked by comparing the fit to the raw data as presented in Fig. 1.

The XAS data analysis program WinXAS 3.1 [41] was used for examining the X-ray absorption near edge structure (XANES) of the samples. Linear combination of the near edge profiles from known reference compounds was used to obtain information about the composition of the samples from different pre-treatment procedures. In order to establish the degree of metallic Au in the samples, the edge profiles were analysed by linear combination of the reference profiles from the Au foil and AuCl. For comparison, linear combinations of the reference profiles from the Au foil and the catalyst sample prior to thermal treatment were also performed.

2.3. WGS activity measurements

The WGS activity measurements were performed in a fixed-bed reactor at atmospheric pressure. The temperature ranged from 190 °C to 310 °C and 100 mg of catalyst was used. The reactor was fed with 50 ml/min CO, 50 ml/min H_2O and 50 ml/min nitrogen. The analytical grade of the gases was 99.999% and no further purification was performed. The product stream was analyzed with an Agilent 3000 micro gas chromatograph. The catalytic activity was calculated from the carbon balance and expressed as the rate of disappearance of CO.

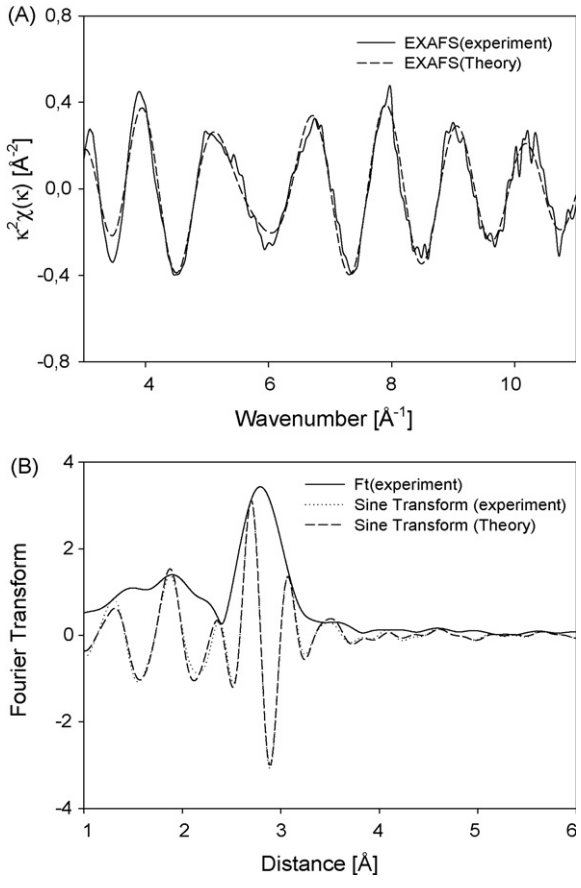

Fig. 1. Experimental and fitted EXAFS data (A) and the corresponding Fourier transform (B) for as-prepared AuCNF_Col.

3. Results and discussion

3.1. Characterisation of the CNF

The CNF were of the fishbone type where the graphite sheets are stacked at an angle with respect to the central axis. The diameter was found to be approximately 50 nm and the concentric walls are regularly spaced by 0.34 nm. The narrow peak observed for the combustion of the CNF in TGA at 630 °C shows that the amount of amorphous carbon is negligible. X-ray diffraction and TEM images (not presented) confirm that the graphite structure is not affected during the acid treatment of the CNF. The BET surface area was determined to be 75 m^2/g.

TGA profiles show that the amount of residue decreased after each purification step. However, the purification method is not able to remove all of the synthesis catalyst. The amount of catalyst in the untreated CNF is approximately 3.6 wt.%. The amount is reduced to 1.2 wt.% after purification. XRF show that the amount of nickel in the samples are between 0.12 wt.% and 0.24 wt.%. Since the original Ni/hydrotalcite catalyst contained 77.5 wt.% nickel, the main component in the residue is alumina. The intensity of the Ni XRD peaks is attenuated for each purification step and the diffractograms show that nickel is present in the metallic phase. Since the nickel is not oxidised it is assumed that nickel is encapsulated in the CNF and will not give any catalytic contribution.

3.2. TiO_2 deposition on CNF

The addition of PEI to $TiCl_4$ has two effects; promotion of the hydrolysis of $TiCl_4$ and as a surfactant. Protonised PEI makes the titania particles positively charged and electro-sterically stabilised. Since the CNF surface is negatively charged the titania can be bound either by amide linkage or through electrostatic attraction [36].

The amount of titania supported on CNF was measured by TGA. The residue after burning of the CNF consists of titania and the residue from the catalyst after preparation of CNF. The amount obtained after subtracting the weight contribution of the derived Ni/hydrotalcite catalyst gave approximately 10 wt.% titania supported on CNF which is the same as the nominal loading. TEM images show that the CNF are not completely covered with oxide (see Fig. 2). The titania particles are covering the CNF as a coating or as clusters attached to the surface. The formation of clusters on parts of the surface instead of an even coating may be because of the insufficient number of surface groups on the CNF surface and that the interactions between the titania particles are stronger than the electrostatic interactions between titania and CNF.

The TiO_2 is predominantly present as anatase since the characteristic XRD diffraction peaks of anatase were evident in each sample. The average TiO_2 crystal size from XRD is

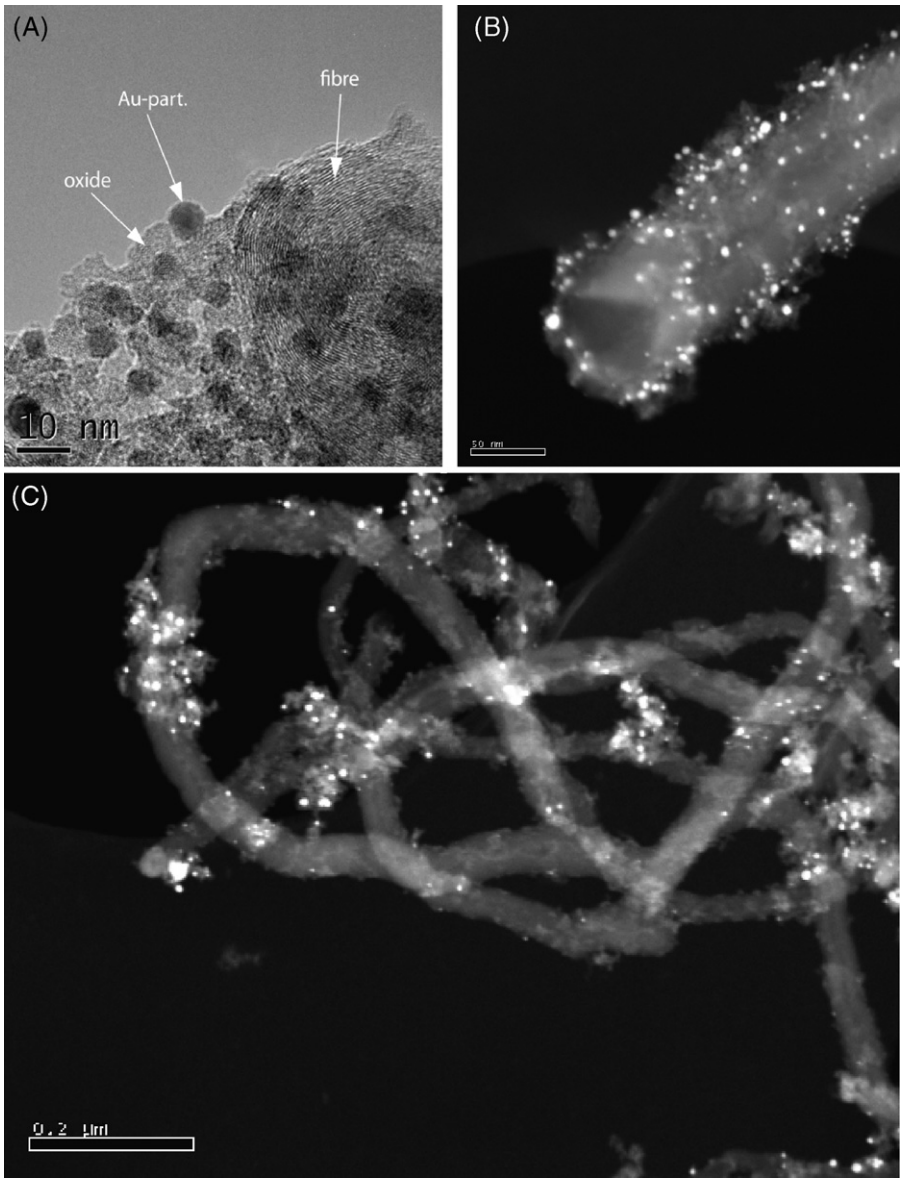

Fig. 2. (A) TEM and (B) STEM images of the samples as-prepared showing Au particles selectively deposited on titania supported on CNF for $AuTiO_2CNF\_Col$. STEM image (C) of the distribution of TiO_2 and Au on the CNF.

approximately 10 nm for both unsupported titania and titania supported on CNF.

Table 1 shows the surface areas and porosities of the support materials. TiO_2 has a larger surface area and lower pore volume compared to CNF and also contains a larger fraction of micropores. The micropores tend to be less stable during thermal treatment and may cause a more rapid deactivation of the catalysts. The CNF contain predominantly mesopores but also a small fraction of micropores. The micropores are probably associated with the hollow core of the CNF. The surface area of CNF increases approximately by 40 m^2/g after deposition of titania. The CNF increase the dispersion of titania and the total pore volume. The amount of micropores is approximately the same as for CNF, which confirms that the hollow core of the CNF is not accessible to the oxide. Since the amount of micropores is unchanged for

Table 1
Surface area and pore volume for the support materials

Sample	Surface area (m^2/g)	Pore volume (cm^3/g)	Micropore surface area (m^2/g)	Micropore volume (cm^3/g)
CNF	75	0.20	10	0.005
TiO_2	114	0.16	70	0.032
TiO_2/CNF	114	0.26	10	0.004

CNF and TiO_2/CNF, the TiO_2 deposited on CNF contains mostly mesopores.

3.3. Deposition from Au colloid solutions

The reduction of chloroauric acid with THPC produced a dark orange-brown sol within a few seconds after mixing. Au colloids in the actual size range have characteristic colours that are highly sensitive to variations in size. The colour of the solution indicates that the Au colloid size is around 2 nm [5,37] and no colour changes could be observed after ageing the solution overnight. This indicates that the solution is stable without growth of the Au particles as reported by Grunwaldt et al. [5]. The Au-sol was characterised by UV–vis and the spectra are presented in Fig. 3. Since their optical properties are very sensitive to aggregation [44] commercial gold colloids with known particle size (5 nm and 10 nm) were investigated for comparison. The colloid solutions of 5 nm and 10 nm exhibit a strong extinction band around 530 nm. The prepared colloid solution with THPC shows only a broad feature around 500 nm. The low intensity of this band corresponds to a gold particle size of about 2 nm [5,14,37].

The deposition of gold colloids was performed at a pH lower than the isoelectric point (IEP) of titania. The isoelectric point of titania was measured to be 5.3 whereas CNF have a negative zeta potential over the entire pH range. The negatively charged gold colloids could hence be selectively adsorbed on the positively charged metal oxide surface. The TEM images of the samples after deposition (Fig. 2) show that the Au particles are deposited selectively on the titania and not on the surface of the CNF. For the Au/CNF sample the particles were deposited directly to the CNF. Since both the Au colloids and CNF are negatively charged the mechanism for deposition is not controlled by electrostatic effects alone. The heterogeneous surface of the carbon, the various surface groups and defects may act as anchoring sites for the gold particles.

High-resolution TEM and STEM reveal that during the preparation procedure, the size of the gold particles is increased compared to the particle size of the original colloid solution.

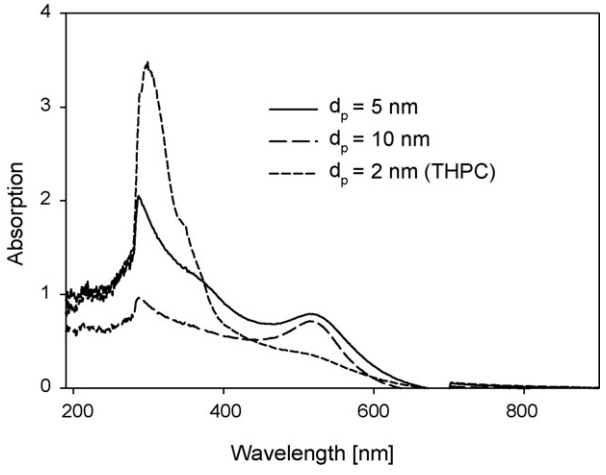

Fig. 3. UV–vis spectra of gold colloid solutions with particle sizes of 2 nm, 5 nm and 10 nm.

Table 2
Comparison of the physical properties of the catalysts

Sample	Au (wt.%)	Cl (wt.%)	Surface area (m^2/g)	Particle size, Au (nm)
AuCNF_Col	1.5[a]	N.D.	75	4.7[c]
$AuTiO_2$CNF_Col	0.9[b]	0.28	111	5.8[c]
$AuTiO_2$_Col	3.3[b]	0.23	110	8.2[c]
AuCNF_DP	2.9[a]	N.D.	64	29[d]
$AuTiO_2$CNF_DP	2.3[a]	N.D.	104	42[d]
$AuTiO_2$_DP	0.5[b]	0.33	109	7.7[c]

N.D., not determined.
[a] Measured by TGA.
[b] Measured by XRF.
[c] Measured by TEM.
[d] Calculated from XRD.

The particle sizes and the amount of Au deposited are reported in Table 2. The fraction of deposited Au decreases in the order TiO_2, CNF and TiO_2/CNF. The difference in loadings is related to the number of surface sites that is available for adsorption of Au.

3.4. Preparation by DP

DP is one of the most frequently used methods for preparing Au based catalysts. TiO_2 can provide both anodic and cathodic sites depending on the pH used in the deposition. Titania is an amphoteric oxide with IEP close to 6 [45]. Titania can hence be used for synthesis by cation adsorption when the pH of the solution is above the IEP and by anion adsorption when the pH is below the IEP. The gold precursor will form complexes in aqueous solution depending on the pH and it is proposed that the first step that occurs during DP of Au on titania is the formation of surface complexes [46]. At pH 2 titania will have a positively charged surface where the main surface species is OH_2^+ whereas the CNF surface will be negative. The adsorption of the negative Au complexes will therefore be selective towards titania at pH below the IEP. This is also observed in the TEM images.

From the Au loadings listed in Table 2 it can be seen that the support materials can retain invariable amounts of Au from the solution. It is not clear if it is the preparation methods that influence the final amount of gold deposited or if some of the gold particles with weak interactions with the support are removed during washing. Zanella et al. [3] have reported that all of the (8 wt.%) gold in the solution is deposited on TiO_2 when using urea but not in the case of NaOH at a final pH of 7. Moreau et al. [11] have shown that the gold uptake goes through a maximum depending on the pH for DP with NaOH. These results are in agreement with a dynamic equilibrium between the adsorbed species and the solution, and that a prolonged preparation time is needed to obtain complete deposition of Au.

The diffractograms of $AuTiO_2$ deposited on CNF prepared by the two methods are presented in Fig. 4. The diffraction peaks for Au(0) are expected at 2θ values of 38.2 (100%), 44.4 (52%), 64.6 (32%) and 77.4 (36%). These peaks are not visible in the XRD patterns except for the samples containing CNF

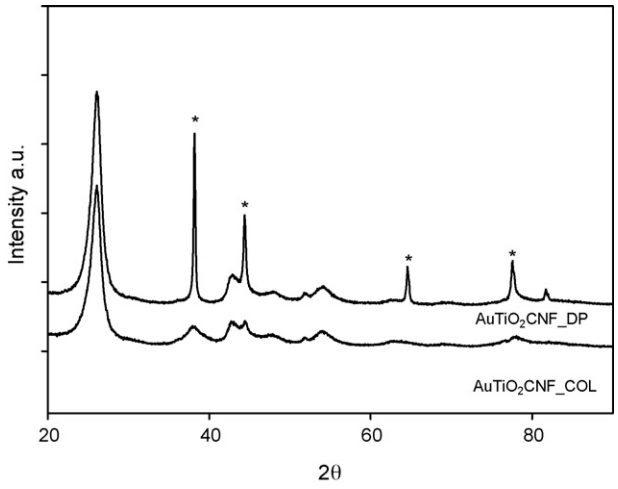

Fig. 4. X-ray diffraction patterns of $AuTiO_2CNF$ prepared by DP and from Au colloid solution. (*) Peaks assigned to Au(0).

made from DP. The absence of the Au peaks in the patterns is because of the small particle size, showing that the DP give significantly larger particle sizes of Au when deposited on CNF and TiO_2/CNF. The average particle size of Au for the samples is given in Table 2. The Au particle size obtained on the various supports increases in the order $TiO_2 < CNF < TiO_2$/CNF for DP. The average Au particle size is larger for $AuTiO_2CNF\_DP$ than for AuCNF_DP. XRD measurements performed prior to and after thermal treatments show a slight increase in particle size for $AuTiO_2CNF\_DP$ from 36 nm to 42 nm and from 25 nm to 29 nm for AuCNF_DP. This confirms that the increase in particle size is more pronounced during the synthesis than during thermal treatment. This increase is observed for the Au particles when CNF is present but not on unsupported TiO_2.

This distinct difference in DP properties suggests that the surface properties of TiO_2 are altered by the CNF. It has been suggested that the curvature of the CNF may introduce strain in nanoparticles deposited on the surface [47]. The low-energy region close to the Ti absorption edge in TiO_2 contains useful information on the local environment of Ti. Experimental and theoretical works have identified four peaks (labelled A1, A2, A3 and B, see Fig. 5) in the pre-edge region of the Ti K-edge XAS spectrum of anatase [48–50]. The A2 peak requires high-resolution detection and is observed as a weak shoulder on the low energy side of the A3 peak. The intensity of the pre-edge A1 and B peaks is sensitive to the local symmetry of the surrounding atoms. They are weak in symmetrical environments and increase in intensity as the environment is distorted [48].

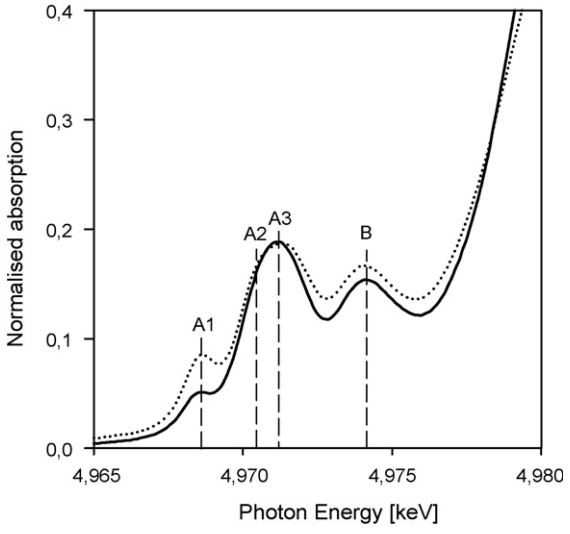

Fig. 5. Ti XANES spectra in the range 4.965–4.980 keV of unsupported TiO_2 and TiO_2 supported on CNF. The features are labelled A1, A2, A3 and B.

Inspection of the XANES spectra in Fig. 5 of TiO_2 and TiO_2 on CNF over a narrow energy range (4.965–4.980) suggests that four pre-edge peaks are present. The intensity of the A2 and A3 peaks are related to the crystallite size [48]. The intensity of the peaks in unsupported and supported TiO_2 is similar, indicating that the particle size of TiO_2 is unchanged when deposited on CNF. The peaks A1 and B are more intense in TiO_2 supported on CNF. The increase in intensity is induced by an increased distortion of the Ti environment. The distortion of the TiO_2 structure is a result of the interaction with the CNF interface. The distorted TiO_2 surfaces obviously suppress the nucleation of Au during DP.

3.5. The valence state of Au in the prepared catalysts

The XRD patterns of the Au based catalysts prepared by DP and supported on CNF show that Au is identified to be in the metallic phase as-prepared. The pre-treatment of the CNF introduce surface functional groups, which can act as anchoring sites for the metals. The oxygen-containing functional groups are involved in the deposition of gold [33]. Since carboxylic and phenolic groups are known to possess redox properties [51,52] they can change the oxidation state of gold without any kind of reduction treatment. Bulushev et al. [33] have demonstrated that the valence state of gold deposited on woven fabrics of activated carbon fibres depends on the type of surface groups. The carboxylic surface groups decompose during interaction with a $[Au(en)_2]Cl_3$ solution to form metallic Au clusters. Interaction of the $[Au(en)_2]Cl_3$ solution with less stable carboxylic groups results in surface decarboxylation and subsequent reduction of Au(III) to Au(0). The Au complexes are deposited on the carboxylic groups, which are more acidic and chemically less stable than the phenolic groups, and hence contribute to the reduction of Au(III). Reduction of Au is also observed for the samples where Au is deposited on titania supported on CNF. Greffiè et al. [53] have identified two forms of gold species on iron oxide after co-precipitation. The formation of gold colloids was attributed to oxidation–reduction reactions between Au(III) and traces of Fe(II). It is very likely that TiO_2 can reduce gold as well since it usually contains defects of Ti^{3+} ions. This indicates that the TiO_2 supported on CNF contains more defects that can promote the reduction of Au(III) than unsupported titania. In addition, the possibility of decomposition of Au(III) during the applied drying conditions due to the redox properties of the support, or even photoreduction of Au by TiO_2 cannot be ruled out.

3.6. Au particle shape

Au particles of different shapes can be observed in the TEM images. Examples of the two shapes are given in Fig. 6. The majority of the particles are hemispherical but polyhedrally faceted particles can also be found in all the catalysts having an average particle size of less than 8 nm (Fig. 6A and B). The shape of the particles seems to be independent of the support material. A notable difference is that the hemispherical particles exhibit a broader size distribution. TEM images of $AuTiO_2$CNF_Col show that the faceted particles are present both before and after the thermal treatment in nitrogen at 300 °C. Haruta [12] have reported that different preparation methods give different Au particle shapes which influence the turnover frequencies for CO oxidation and that the Au particles prepared by DP had a hemispherical shape, with their flat crystallite faces strongly attached to the TiO_2. This suggests that there are variations in the interaction strength between the support and the Au particles, giving rise to different Au particle shapes. Lopez et al. [54] have performed density-functional theory (DFT) calculations for gold on a rutile TiO_2(1 1 0) surface. They claim that the adhesion energy for gold particles on a perfect TiO_2 surface is negligible and that defects are required to obtain stable gold particles. The final size and shape of the gold particles is determined by the interface energy between Au and TiO_2. Oxygen defects in the support material will therefore contribute to determining the shape of gold particles.

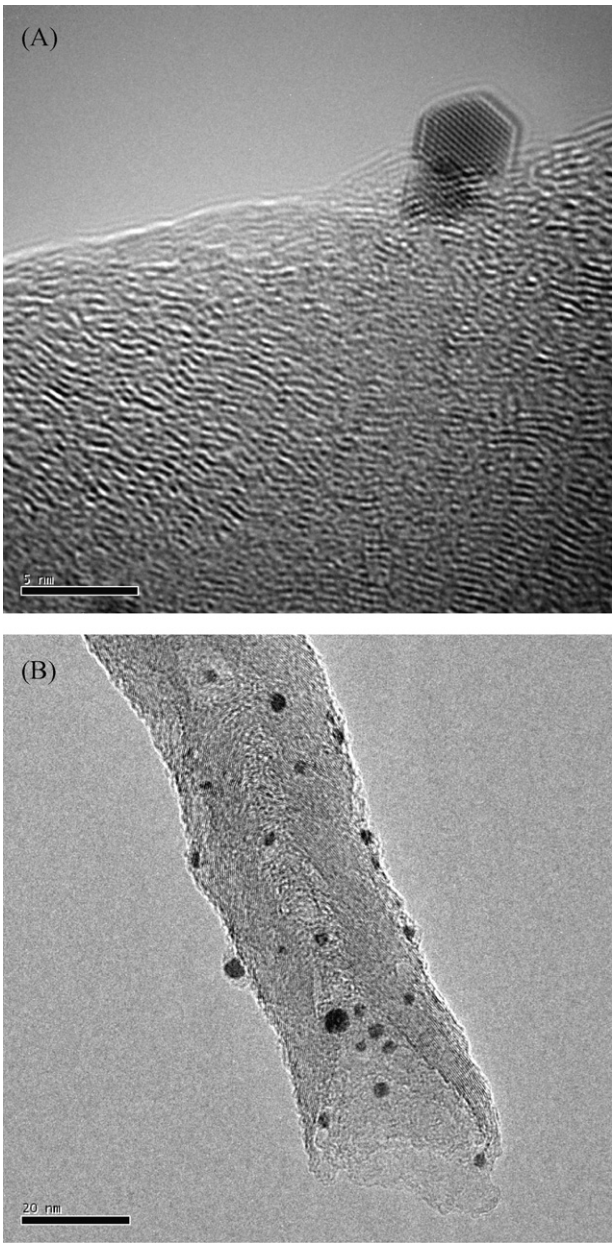

Fig. 6. TEM/HAADF STEM images of AuCNF_Col showing (A) a 5 nm polyhedral faced particle and (B) particles with various shapes supported on CNF.

3.7. Pre-treatments

XANES provides information about the oxidation states and site symmetries of the gold species. An *in situ* XAS study of the pre-treatment of the samples was performed. Linear combination of the edge profiles was performed using Au(0) (Au metal) and Au(I) (AuCl) as reference compounds to determine the distribution of valence states in the catalysts. No evidence of Au(III) could be detected in any of the samples before or during the different treatments. The fraction of Au(I) decreases for both $AuTiO_2$/CNF_Col and Au/CNF_Col with increasing temperature. This is reflected in the results from the linear combination of XANES presented in Fig. 7 (Au/CNF_Col) and

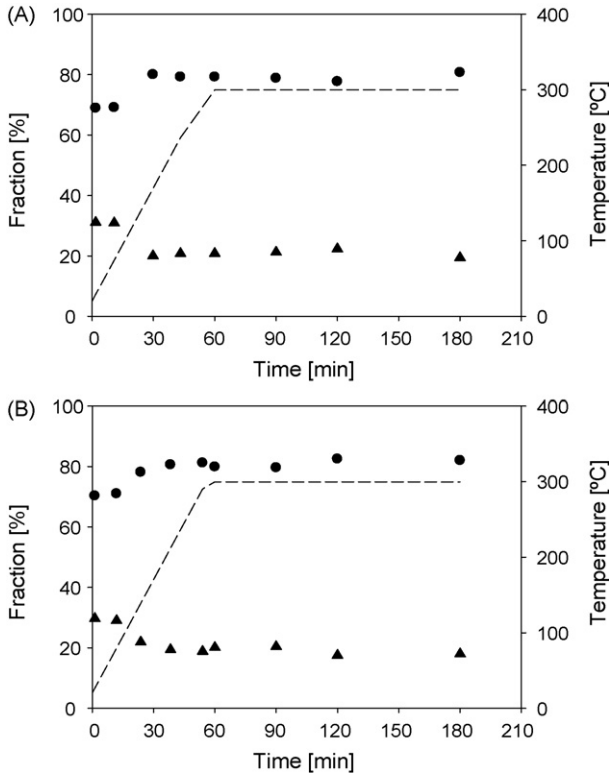

Fig. 7. Fractions of Au(0) (circle) and Au(1) (triangles) obtained from linear combination of XANES spectra during different pre-treatments of AuCNF_Col; (A) treated in 5% O_2/He and (B) treated in He. The temperature is plotted as a dashed line.

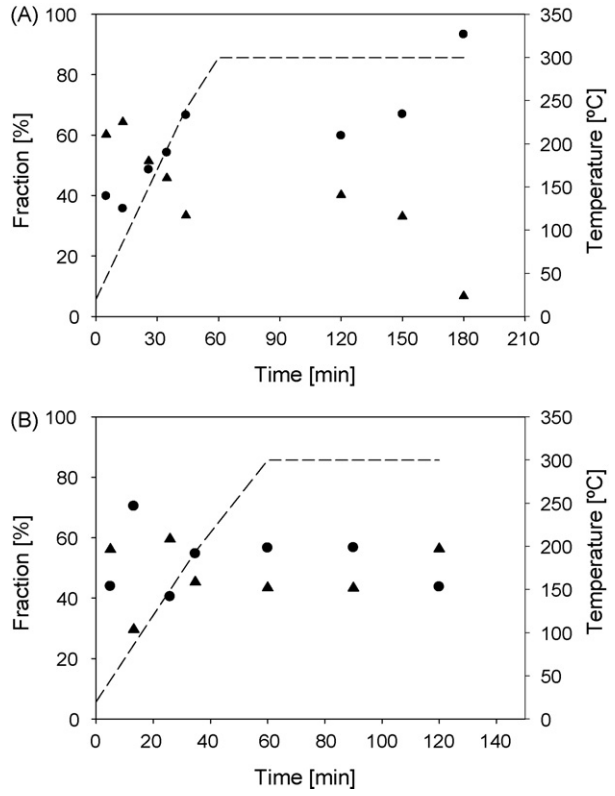

Fig. 8. Fractions of Au(0) (circle) and Au(I) (triangles) obtained from linear combination of XANES spectra during different pre-treatments of $AuTiO_2$CNF_Col; (A) treated in 5% O_2/He followed by (B) reduction in 5% H_2/He. The temperature is plotted as a dashed line.

Fig. 8 ($AuTiO_2$/CNF_Col). The changes in valence states for Au/CNF_Col are similar in oxygen and helium. Since the fraction of metallic Au is increasing with the same fraction in both gases it is likely that the changes observed are because of structural changes and rearrangements of the cluster-support induced by the thermal treatment.

Partial oxidation (10%) of small gold particles (<30 Å) have been reported and identified as Au(III), whereas larger particles were not noticeably oxidised [55]. Since only Au(0) and Au(I) can be observed, oxidation of gold particles is not a likely explanation for the valence shift in the present samples. Tibiletti et al. [56] have performed EXAFS and XANES experiments and DFT calculations and are suggesting a model where a metallic gold cluster containing about 50 atoms is in intimate contact with the oxide support to the extent that up to 15% of the gold atoms at the interface with the support may be located at cation vacancies. Such gold atoms would be expected to carry a small positive charge. This is in agreement with the positive charge that is observed in the XANES spectra being a result of gold–support interactions. However, it is clear that metallic gold is the main constituent in the samples from both synthesis methods.

The fraction of Au(I) is larger for $AuTiO_2$/CNF_Col than for Au/CNF_Col. This is because the average particle size is smaller for $AuTiO_2$/CNF_Col, where a larger fraction of atoms is located at the metal–support interface where cationic gold is stabilised by the support. This indicates that titania has a stronger interaction with the Au particles than carbon. However, during heating in oxygen the fraction of metallic gold in $AuTiO_2$/CNF_Col increases as well and after 2 h the total fraction of Au(0) is larger than for Au/CNF_Col. Purging the sample in helium followed by introduction of H_2/He immediately results in changes in the fraction of Au(I). The fraction of Au(I) increases to approximately 45% and is relatively constant during the treatment. The relatively large change in oxidation states for Au can be a combination of structural changes and adsorption of hydrogen on the surface. Note that the Au(I) fraction is merely an expression of the partial positive charge on the Au atoms ($Au^{\delta+}$) rather than of a formal oxidation state. The charge is reflected in the shift of the L_{III} absorption edge energy. *In situ* XAS studies show that the WGS activity is higher when the fraction of $Au^{\delta+}$ is high, although the positive charge during WGS can arise from CO (or hydrogen) chemisorption on Au or by dynamic changes in the metal–support interaction [57]. Bus et al. [58] have demonstrated that hydrogen adsorbs dissociatively on the gold atoms of Au/Al_2O_3 and that the dissociation of H_2 is limited to gold atoms at corner and edge positions. Exposing the Au/Al_2O_3 to H_2 induced a change in the Au L_{III} and L_{II} XANES, which were used to identify hydrogen-binding sites on supported gold catalysts. Since titania is a partially reducible oxide, hydrogen may create vacancies in the oxide structure that are able to promote the interaction with gold particles.

The fitted EXAFS spectrum of AuCNF_Col from the *in situ* treatment in oxygen is presented in Fig. 1 together with the corresponding Fourier transform. The parameters obtained from the EXAFS analysis are summarised in Table 3. The coordination number for the first Au–Au shell is lower than for the fcc structure, which has a coordination number of 12. The reduced coordination numbers and the contraction of the interatomic distances are consistent with the presence of small gold particles. A maximum contraction of about 0.15 Å for the Au–Au distance has been reported for catalysts with close to 100% dispersion (corresponding to an approximate particle size of 1 nm) [55].

The Au–Au coordination number increases after thermal treatment in oxygen and helium. This is in agreement with what Guzman and Gates [59] have reported for thermal treatment in helium and hydrogen at different temperatures for Au supported on MgO. Their results show that the coordination numbers for the first and second Au–Au shell are systematically

Table 3
Results from *in situ* EXAFS analysis for $AuTiO_2$CNF_Col and AuCNF_Col treated in different gases

Sample	Gas	Before			After		
		N^a	R^b (Å)	$2\sigma^{2\,c}$	N^a	R^b (Å)	$2\sigma^{2\,c}$
$AuTiO_2$/CNF_Col	5% O_2/He	9.4	2.86	0.015	11.7	2.86	0.017
$AuTiO_2$/CNF_Col	5% H_2/He	9.4	2.86	0.015	11.0	2.85	0.017
Au/CNF_Col	5% O_2/He	8.3	2.83	0.019	9.6	2.85	0.014
Au/CNF_Col	He	8.3	2.83	0.019	9.8	2.85	0.014

[a] First Au–Au coordination number, *N*: ±20%.
[b] Interatomic distance, *R*: ±0.02 Å.
[c] Debye–Waller type factor.

increasing from 1.1 to 9.4 in the temperature range of 323–573 K. They used [$Au(CH_3)_2(acac)$] as a precursor and the increase in coordination number can therefore be explained by migration and aggregation of Au on the MgO surface. The increase in the Au–Au coordination number in the present work could also be a result of contaminants such as residual chloride together with migration and agglomeration of the Au particles. Oxidation followed by reduction of $AuTiO_2$/CNF_Col causes no further increase in coordination number and the Au–Au interatomic distance. This suggests that the oxygen treatment leads to stronger interaction between the gold particles and the TiO_2 and prevents further particle sintering. Zanella and Louis [60] claim that the particle growth deceases when the gas flow is increased, when the amount of sample decreases or when H_2 or Ar is used instead of air. The two first parameters had a stronger effect on the particle size than the treatment temperature. The coordination numbers obtained for Au/CNF_Col in the present work after treatment in oxygen and in He is approximately the same suggesting that temperature is the decisive factor. Note that the concentration of oxygen used in this work is lower and the average particle size larger than in the work reported by Zanella and Louis [60] making the observations not directly comparable.

No Au–Cl coordination can be detected in the EXAFS spectra for any of the samples. This contribution is not expected to be found in samples prepared by deposition from colloid solutions since the Au complexes are reduced in the solution. However, the Au–Cl coordination was not detectable in the samples prepared by DP. Since XRF results (see Table 2) show that a significant residue of Cl^- is present in the samples it is most likely located at the support. A minor Au–C or Au–O contribution could be identified in some of the spectra, but was too weak to give any reliable information. Miller et al. [55] have reported that the Au–O peaks are small and are partially overlapping the larger Au–Au contribution. This makes it difficult to deconvolute and extract the parameters for the metal–support interaction.

TEM images have been acquired for $AuTiO_2$/CNF_Col prior to and after thermal treatment in nitrogen at 300 °C for 2 h. The gold particle size distributions are given in Fig. 9. The Au particles in the untreated sample are relatively small and the majority are in the range of 2–5 nm, although there is also a fraction of larger particles in the range of 10–20 nm. In the sample subjected to thermal treatment the majority of the particles are 3–10 nm, with a significant fraction being larger than 5 nm. The presence of residual Cl^- species from the precursor may initiate agglomeration of gold particles [61]. The agglomeration of the gold particles after thermal treatment is independent of preparation method and can be observed for all the catalysts. Estimating particle size from XRD is difficult since the diffraction peaks from gold are overlapping with peaks from the other components in the catalysts. A significant effect of thermal treatment on the growth of gold particles is observed. However, the titania particle size remains unchanged, indicating that the titania particles are more stable during thermal treatment than the gold particles.

3.8. The water–gas shift reaction

The catalysts are active for the WGS reaction in the temperature range of 190–300 °C. Fig. 10 shows the reaction rates as a function of temperature. The $AuTiO_2$/CNF catalyst prepared by DP was not tested for catalytic activity. TEM images show that this sample is dominated by gold particles in the range of 100–200 nm, which are not active. The activity of Au supported on CNF alone is very low and the presence of titania significantly increases the catalytic activity. WGS activity measurements of CNF have been performed and the material did not show any observable activity at the current conditions. Bollinger and Vannice [62] argue that the active sites for CO oxidation are located at the Au–TiO_2 interface creating a synergy effect between TiO_2 and Au. The WGS reaction is proposed to follow a mechanism involving a partially reducible oxide and metal particles. The role of the oxide in such systems is proposed to be via an oxide-mediated redox process where the oxide reducibility (or oxygen storage capacity) and the metal particles are the active elements [30]. The bifunctional nature of the reaction is reflected in the present WGS activity measurements, which show that both the Au

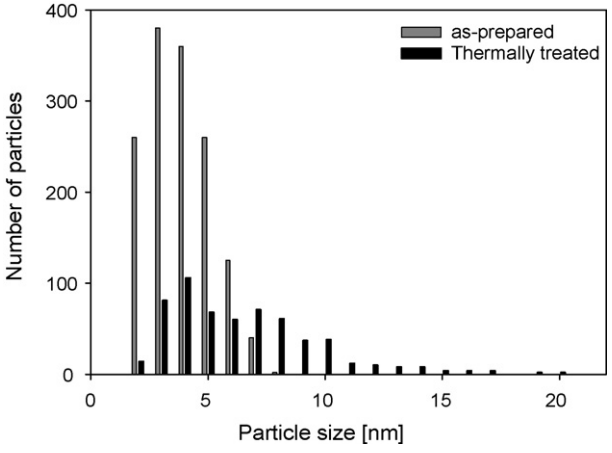

Fig. 9. Size distribution of $AuTiO_2$CNF_Col as-prepared (grey) and thermally treated at 250 °C in nitrogen for 1 h (black).

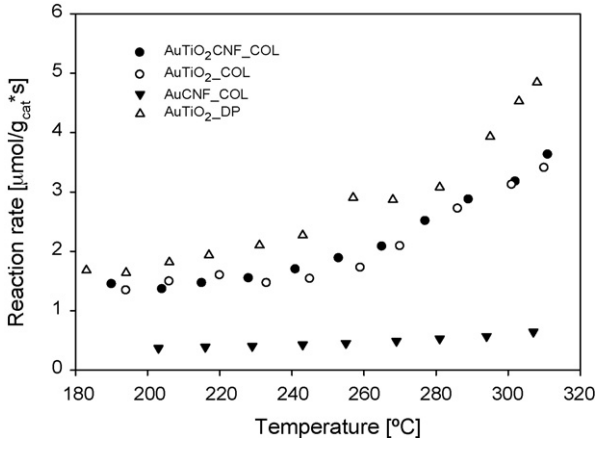

Fig. 10. Water–gas shift reaction rates as a function of temperature.

Table 4
Au dispersion and turnover frequencies for the catalyst samples

Sample	Au dispersion[a]	TOF (s^{-1}) at 310 °C
AuCNF_Col	19.1	0.04
$AuTiO_2$CNF_Col	15.5	0.4
$AuTiO_2$_Col	11.0	0.2
AuCNF_DP	3.1	–
$AuTiO_2$CNF_DP	2.1	–
$AuTiO_2$_DP	11.7	1.6

[a] The dispersion is calculated from the average particle size ($D = 0.9/d_p$).

particles and the oxide have to be present in order to obtain high activity.

DP gives a higher reaction rate for Au deposited on titania than the colloid preparation route. The average Au particle size in the two samples is comparable although $AuTiO_2$_Col has a higher Au loading. The Au dispersion and the turnover frequencies (TOF) of the catalysts are presented in Table 4. The dispersion is estimated from the mean particle size. The $AuTiO_2$_DP and $AuTiO_2$_Col have similar dispersion. However, the TOF is eight times higher for the catalyst prepared by DP. This shows that DP introduces more favourable structural properties on the Au particles compared to colloids. Moreover, it indicates that the catalysts prepared from colloids require different pre-treatment procedures to obtain high activity.

Although $AuTiO_2$CNF_Col and $AuTiO_2$_Col show similar reaction rate per gram catalyst in Fig. 10, the specific rates are different. The TOF of $AuTiO_2$CNF_Col is higher than for $AuTiO_2$_Col, which contains significantly larger particles. This can be due to the particle size distribution in $AuTiO_2$_Col where a significant fraction of the gold particles are too large to contribute to the catalytic activity. The results suggest that the reaction is structure sensitive and that smaller Au particles lead to higher turnover frequencies. Since TiO_2 contribute to the activity, the distortion of the TiO_2 structure by the CNF may also introduce changes that promote the TOF.

Recent studies comparing Au on TiO_2CNF with Au on a commercial TiO_2 support of lower surface area indicate that the TiO_2 on CNF is relatively amorphous and hence contains more defects than the crystalline support [57]. The beneficial effect of the CNF is less evident in the present study when $AuTiO_2$CNF is compared to Au on TiO_2 of comparable surface area. Furthermore, other factors such as particle size and shape seem to give a more significant contribution to the catalytic activity.

4. Conclusions

The nature of the Au nanoparticles obtained from DP and colloid solutions, respectively, is highly depending on the support material they are deposited on. DP yields large Au particles (>50 nm) on CNF supports and on titania/CNF. Finely dispersed Au particles are only obtained when deposited on unsupported TiO_2. To maintain high dispersion on carbon nanofibres the Au precursor must be converted to the metallic form as part of the initial preparation, i.e. via colloid formation. This is due to the redox properties of the CNF which causes reduction of Au(III) to Au(0) during adsorption, which creates nucleation points leading to larger particle sizes. Au particles can be selectively deposited on the oxide surface due to the reverse polarity of the CNF and TiO_2 surfaces at given pH values.

The increase in particle size is more pronounced during the DP synthesis steps than in the thermal treatments. This increase is observed for the Au particles on TiO_2 only when CNF is present. The TiO_2 XANES analyses show that distortions in the lattice symmetry of TiO_2 are introduced when the oxide is deposited on CNF.

The WGS activity significantly improves when titania is present in the catalytic material compared to deposition of Au directly on CNF. This shows that high catalytic activity in the water–gas shift reaction is obtained only when both Au and the oxide are present, indicating that the active sites are either on the Au–TiO_2 interface or that the reaction follows a bifunctional mechanism. The TOF is eight times higher for the Au/TiO_2 catalyst prepared by DP. This shows that DP introduces more favourable structural properties on the Au particles compared to colloids.

The specific rates of the catalysts prepared from colloids suggest that the reaction is structure sensitive and that smaller Au particles lead to higher turnover frequencies. The distortion of the TiO_2 structure by the CNF may also introduce changes that promote the TOF.

Acknowledgements

We acknowledge the project teams at the Swiss-Norwegian Beam Lines (SNBL) at ESRF and at Beam Line 11.1, ELETTRA, Trieste, Italy, S.C.p.A. for their assistance. The Norwegian University of Science and Technology (NTNU) and The Research Council of Norway (Grant no. 158516/510, NANOMAT) are acknowledged for financial support.

References

[1] M. Haruta, S. Tsubota, T. Kobayashi, H. Kageyama, M.J. Genet, B. Delmon, J. Catal. 144 (1993) 175.
[2] Q. Fu, S. Kudriavtseva, H. Saltsburg, M. Flytzani-Stephanopoulos, Chem. Eng. J. 93 (2003) 41.
[3] R. Zanella, S. Giorgio, C.-H. Shin, C.R. Henry, C. Louis, J. Catal. 222 (2004) 357.
[4] Q. Xu, K.C.C. Kharas, A.K. Datye, Catal. Lett. 85 (2003) 229.
[5] J.-D. Grunwaldt, C. Kiener, C. Wögerbauer, A. Baiker, J. Catal. 181 (1999) 223.
[6] F. Porta, M. Rossi, J. Mol. Catal. A: Chem. 204–205 (2003) 553.
[7] S. Hannemann, J.-D. Grunwaldt, F. Krumeich, P. Kappen, A. Baiker, Appl. Surf. Sci. 252 (2006) 7862.
[8] G.B. Hoflund, S.D. Gardner, D.R. Schryer, B.T. Upchurch, E.J. Kielin, Appl. Catal. B 6 (1995) 117.
[9] M. Haruta, N. Yamada, T. Kobayashi, S. Iijima, J. Catal. 115 (1989) 301.
[10] S. Tsubota, D.A.H. Cunningham, Y. Bando, M. Haruta, Stud. Surf. Sci. Catal. 91 (1995) 227.
[11] F. Moreau, G.C. Bond, A.O. Taylor, J. Catal. 231 (2005) 105.
[12] M. Haruta, Cattech 6 (2002) 102.
[13] J. Turkevich, P.L. Stevenson, J. Hillier, Discuss. Faraday Soc. 11 (1951) 55.
[14] D.G. Duff, A. Baiker, P.P. Edwards, Langmuir 9 (1993) 2301.

[15] D.G. Duff, A. Baiker, I. Gameson, P.P. Edwards, Langmuir 9 (1993) 2310.
[16] G.C. Bond, D.T. Thompson, Catal. Rev. Sci. Eng. 41 (1999) 319.
[17] H. Sakurai, A. Ueda, T. Kobayashi, M. Haruta, Chem. Commun. (1997) 271.
[18] V. Idakiev, T. Tabakova, Z.-Y. Yuan, B.-L. Su, Appl. Catal. A 270 (2004) 135.
[19] F. Boccuzzi, A. Chiorino, M. Manzoli, D. Andreeva, T. Tabakova, L. Ilivers, V. Idakiev, Catal. Today 75 (2002) 169.
[20] T. Tabakova, V. Idakiev, D. Andreeva, I. Mitov, Appl. Catal. A 202 (2000) 91.
[21] V. Idakiev, T. Tabakova, A. Naydenov, Z.-Y. Yuan, B.-L. Su, Appl. Catal. B 63 (2006) 178.
[22] T. Tabakova, F. Boccuzzi, M. Mzoli, J.W. Sobczak, V. Idakiev, D. Andrevva, Appl. Catal. B 49 (2004) 73.
[23] G. Jacobs, P.M. Patterson, L. Williams, E. Chenu, D. Sparks, G. Thomas, B.H. Davis, Appl. Catal. A 262 (2004) 177.
[24] A. Venugopal, M.S. Scurrell, Appl. Catal. A 258 (2004) 241.
[25] S.T. Daniells, M. Makkee, J.A. Moulijn, Catal. Lett. 100 (2005) 39.
[26] Q. Fu, W. Deng, H. Saltsburg, M. Flytzani-Stephanoloulos, Appl. Catal. B 56 (2005) 57.
[27] Q. Fu, H. Saltsburg, M. Flytzani-Stepanopoulos, Science 301 (2003) 935.
[28] G. Jacobs, E. Chenu, P.M. Patterson, L. Williams, D. Sparks, G. Thomas, B.H. Davis, Appl. Catal. A 258 (2004) 203.
[29] D. Andreeva, V. Idakiev, T. Tabakova, A. Andreev, J. Catal. 158 (1996) 354.
[30] Q. Fu, A. Weber, M. Flytzani-Stephanopoulos, Catal. Lett. 77 (2001) 87.
[31] H. Sakurai, T. Akita, S. Tsubota, M. Kiuchi, M. Haruta, Appl. Catal. A 291 (2005) 179.
[32] P. Serp, M. Corrias, P. Kalck, Appl. Catal. A 253 (2003) 337.
[33] D.A. Bulushev, I. Yuranov, E.I. Suvorova, P.A. Buffat, L. Kiwi-Minsker, J. Catal. 224 (2004) 8.
[34] L. Prati, F. Porta, Appl. Catal. A 291 (2005) 199.
[35] Z. Yu, D. Chen, B. Tøtdal, A. Holmen, Mater. Chem. Phys. 92 (2005) 71.
[36] J. Sun, M. Iwasa, L. Gao, Q. Zhang, Carbon 42 (2004) 885.
[37] D.G. Duff, A. Baiker, P.P. Edwards, J. Chem. Soc., Chem. Commun. (1993) 96.
[38] D. Bom, R. Andrews, D. Jacques, J. Anthony, B. Chen, M.S. Meier, J.P. Selegue, Nano Lett. 2 (2002) 615.
[39] DTS Customer Training Manual, Chapter 6, Zeta Potential Theory, p. 66.
[40] F.W. Lytle, R.B. Greegor, E.C. Marques, D.R. Sandstrom, G.H. Via, J.H. Sinfelt, J. Catal. 95 (1985) 546.
[41] T.J. Ressler, J. Phys. IV C2 (1997).
[42] EXCURV98 CCLRC Daresbury Laboratory computer program.
[43] S.J. Gurman, N. Binsted, I. Ross, J. Phys. C 17 (1984) 143.
[44] P. Mulvaney, Langmuir 12 (1996) 788.
[45] M. Kosmulski, J. Colloid Interf. Sci. 298 (2006) 730.
[46] M. Haruta, Catal. Today 36 (1997) 153.
[47] E. Ochoa-Fernàndez, D. Chen, Z. Yu, B. Tøtdal, M. Rønning, A. Holmen, Surf. Sci. 554 (2004) L107.
[48] V. Luca, S. Djajanti, R.F. Howe, J. Phys. Chem. B 102 (1998) 10650.
[49] S.J. Stewart, M. Fernández-Garcia, C. Belver, B.S. Mun, F.G. Requejo, J. Phys. Chem. B 110 (2006) 16482.
[50] R. Brydson, H. Sauer, W. Engel, J.M. Thomas, E. Zeitler, N. Kosugi, H. Kurodal, J. Phys.: Condens. Matter 1 (1989) 797.
[51] E. Auer, A. Freund, J. Pietsch, T. Tacke, Appl. Catal. A 173 (1998) 259.
[52] D.S. Cameron, S.J. Copper, I.L. Dodgson, B. Harrison, J.W. Jenkins, Catal. Today 7 (1990) 113.
[53] C. Greffiè, M.F. Benedetti, C. Parron, M. Amouric, Geochim. Cosmochim. Acta 60 (1996) 1531.
[54] N. Lopez, J.K. Nørskov, T.V.W. Janssens, A. Carlsson, A. Puig-Molina, B.S. Clausen, J.-D. Grunwaldt, J. Catal. 225 (2004) 86.
[55] J.T. Miller, A.J. Kropf, Y. Zha, J.R. Regalbuto, L. Delannoy, C. Louis, E. Bus, J.A. van Bokhoven, J. Catal. 240 (2006) 222.
[56] D. Tibiletti, A. Amieiro-Fonseca, R. Burch, Y. Chen, J.M. Fisher, A. Goguet, C. Hardacre, P. Hu, D. Thompsett, J. Phys. Chem. B 109 (2005) 22553.
[57] N. Hammer, I. Kvande, W. van Beek, D. Chen, M. Rønning, Top. Catal. (2007), doi:10.1007/s11244-007-0235-6.
[58] E. Bus, J.T. Miller, J.A. van Bokhoven, J. Phys. Chem. B 109 (2005) 14581.
[59] J. Guzman, B.C. Gates, Nano Lett. 1 (2001) 689.
[60] R. Zanella, C. Louis, Catal. Today 107–108 (2005) 768.
[61] H.-S. Oh, J.H. Yang, C.K. Costello, Y.M. Wang, S.R. Bare, H.H. Kung, M.C. Kung, J. Catal. 210 (2002) 375.
[62] M.A. Bollinger, M.A. Vannice, Appl. Catal. B 8 (1996) 417.